Mon. Not. R. Astron. Soc. **321**, L15–L19 (2001)

Chandra detection of reflected X-ray emission from the type 2 QSO in IRAS 09104+4109

K. Iwasawa,★ A. C. Fabian and S. Ettori
Institute of Astronomy, Madingley Road, Cambridge CB3 0HA

Accepted 2000 November 23. Received 2000 November 23; in original form 2000 October 9

ABSTRACT

We present X-ray imaging spectroscopy of the extremely luminous infrared galaxy IRAS 09104+4109 ($z = 0.442$) obtained with the *Chandra* X-ray Observatory. With the arcsec resolution of *Chandra*, an unresolved source at the nucleus is separated from the surrounding cluster emission. A strong iron K line at 6.4 keV on a very hard continuum is detected from the nuclear source, rendering IRAS 09104+4109 the most distant reflection-dominated X-ray source known. Combined with the *BeppoSAX* detection of the excess hard X-ray emission, it provides further strong support for the presence of a hidden X-ray source of quasar luminosity in this infrared galaxy. Also seen is a faint linear structure to the north, which coincides with the main radio jet. An X-ray deficit in the corresponding region suggests an interaction between the cluster medium and the jet driven by the active nucleus.

Key words: galaxies: individual: IRAS 09104+4109 – infrared: galaxies – X-rays: galaxies.

1 INTRODUCTION

IRAS 09104+4109 (FSC 09105+4108) is one of the extremely luminous infrared galaxies detected in the *IRAS* survey and has been considered to be a dust-enshrouded type 2 QSO (Kleinmann et al. 1988; Hines & Wills 1993; Crawford & Vanderriest 1996; Granato, Danese & Franceschini 1996; Soifer et al. 1996; Taniguchi et al. 1997; Evans et al. 1998; Hines et al. 1999; Franceschini et al. 2000; Tran, Cohen & Villar-Martin 2000). The infrared source ($L_{\rm ir} \simeq 6 \times 10^{12}\, h^{-2}\, {\rm L}_{\odot}$)[1] has been identified with a cD galaxy in a rich cluster at a redshift of 0.442 (Kleinmann et al. 1988). Extended X-ray emission was detected with the *ROSAT* HRI, and has been identified with the intracluster medium (ICM), in which a strong cooling flow is taking place (Fabian & Crawford 1995; Crawford & Vanderriest 1996; Allen & Fabian 1998). Although the cluster emission itself is of great interest, it makes an X-ray investigation of the active nucleus difficult for X-ray telescopes with a relatively low spatial resolution like *ASCA* (e.g. Fabian et al. 1994) and even *XMM*. The first X-ray evidence for a luminous active nucleus came from an observation in the hard X-ray band where cluster emission is negligible. The detection of a hard X-ray excess with *BeppoSAX*, although its significance is marginal (3σ) and subject to possible contaminating sources in the large field of view of the Phoswich Detector System (PDS) detector (Frontera et al. 1997), suggests a strongly absorbed nucleus (Franceschini et al. 2000). The other way to access the active nucleus is to utilize a high spatial resolution to separate the nucleus from the diffuse emission in an appropriate energy range. With the 1-arcsec resolution of the X-ray telescope (Weisskopf, O'Dell & van Speybroeck 1996) and the Advanced CCD Imaging Spectrometer (ACIS) CCD detectors, *Chandra* overcomes the difficulty. In this Letter, we present the spatially resolved X-ray source associated with the nucleus of IRAS 09104+4109 and its spectral properties.

2 OBSERVATION AND DATA REDUCTION

IRAS 09104+4109 was observed with the *Chandra* X-ray Observatory on 1999 November 3. The galaxy was positioned near the aimpoint of ACIS-S3, which was operating in Faint mode. Events with the *ASCA* grade of 0, 2, 3, 4 and 6 were selected. The background of the ACIS-S3 chip remained within a factor of 2 of the mean count rate most of the time, but flared occasionally by up to a factor of 4. We have discarded the periods of unusually high background events for the data of extended emission, which left a total of 8.4 ks exposure. For a spectrum of the nuclear point source extracted from a small region of the detector, we consider the background variation to have no effect and used the full exposure of 9.1 ks.

The data were reduced using software in CIAO 1.1.4 with the most up-to-date calibration available from the *Chandra* Science Center. The temperature of the focal plane detector is estimated to be -110°C, and an appropriate Fits Embedded Function (FEF) file is selected accordingly in making the response matrix. The energy resolution of the spectrum above 3.5 keV is about 3 per cent (or ~140 eV at 4.5 keV where a Fe K line is expected for the

★ E-mail: ki@ast.cam.ac.uk

[1] $H_0 = 100\, h\, {\rm km\, s^{-1}\, Mpc^{-1}}$ and $q_0 = 0.5$ are assumed throughout this paper.

redshift of the galaxy) at FWHM. X-ray spectra were extracted from the `PI` column and relevant response matrices were created by `mkrmf` and `mkarf`. A spectral analysis was performed using XSPEC version 11.

3 RESULTS

3.1 X-ray image

The full-resolution raw image (1 pixel $\sim$ 0.5 arcsec) of the central part of IRAS 09104+4109 in the 0.5–8 keV band is shown in Fig. 1. A bright point-like source is seen in the middle of the X-ray image surrounded by extended emission of an irregular shape. The image profile of the bright source is consistent with the point spread function. This point-like nature becomes clearer in the high-energy band (e.g. 3–8 keV) image, in which most of the source photons are concentrated within 2 pixels in radius. The radial profile of the hardness ratios demonstrate the distinctly hard spectrum of the nuclear source (Fig. 2).

The position of the point source is located at $\sim$1.5 arcsec to the south-west of the radio core measured by Hines & Wills (1993), which we believe is due to an inaccurate aspect solution in the *Chandra* data. Notable is a faint linear feature at $\sim$10 arcsec from the point source extending to the north-north-west (at a position angle of $\sim$340°). The feature points to the bright central source and, assuming the central source to coincide with the active nucleus, it matches the radio structure of the preceding north radio lobe and hot spot, found in the Very Large Array (VLA) images (Kleinmann et al. 1988; Hines & Wills 1993). However, this X-ray feature is very faint and it is difficult to assess its significance because of the non-uniform background of the complex cluster emission (about 2σ excess compared with the surroundings). Our estimate of the flux at 1 keV from the jet is $(3 \pm 2) \times 10^{-15}$ erg cm^{-2} s^{-1}, more than an order of magnitude above the radio power measured with VLA (Hines & Wills 1993). The radio jet is believed to emanate close to the plane of the sky and its bulk velocity is $\sim 0.1c$ (Hines et al. 1999). No detection of an optical jet is reported. This X-ray feature could be Compton-upscattered photons of beamed radiation from the nucleus in the mildly relativistic electrons (Celotti, Ghisellini & Chiaberge 2001).

It should also be noted that the north-west quarter of the inner part of the extended emission is significantly lower in X-ray surface brightness than the rest, by 30–40 per cent. This X-ray deficit was probably viewed as a 'hole' in the *ROSAT* HRI image (Fabian & Crawford 1995; Crawford & Vanderriest 1996). Since this region lies along the direction of the radio/X-ray jet, it is plausible that the ICM has been affected by the jet and thus the low surface brightness region is similar to the X-ray cavities seen also by *Chandra* in other clusters harbouring a strong radio source in their centre (e.g. the Hydra A cluster, McNamara et al. 2000; the Perseus cluster, Fabian et al. 2000a). However, it is interesting to note the relatively wide opening angle ($\sim$90°) of the cavity despite the rather slim radio jet in IRAS 09104+4109. The optical emission plume (Kleinmann et al. 1988; Hutchings & Neff 1988; Soifer et al. 1996; Crawford & Vanderriest 1996; Armus, Soifer & Neugebauer 1999; Tran et al. 2000) is located at the edge of this X-ray cavity and a strongly blueshifted component of emission-line gas at the nucleus, supporting the idea of a central outflow.

Here, we mention the cluster emission briefly, and further details will appear elsewhere. The large-scale X-ray envelope is elongated along the east–west direction, which is consistent with the flattened galaxy distribution of the cluster (Kleinmann et al. 1988), while the X-ray morphology of the inner part is more complex. A significant radial temperature gradient is found: the temperature of 7.8 ± 1.5 keV found at radii of 200 kpc drops to 3.3 ± 0.3 keV near the nucleus, when fitted to a single-temperature thermal emission model. This clearly indicates that strong cooling of the ICM is taking place in the dense core of the cluster, as previously suggested from the X-ray imaging and spectral analysis (Fabian & Crawford 1995; Allen & Fabian 1998; Ettori & Fabian 1999).

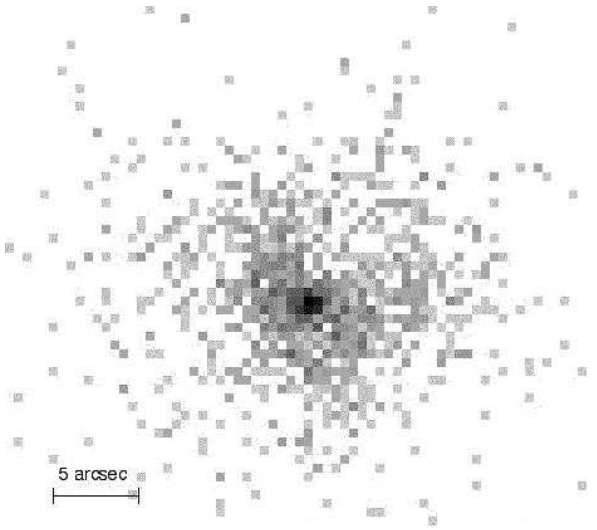

Figure 1. The 0.5–8 keV image of IRAS 09104+4109 obtained from the *Chandra* X-ray Observatory ACIS-S3. The unsmoothed full-resolution image is presented with a logarithmic scale. In the image, north is up, east is to the left, and an angular scale of 5 arcsec is indicated. The brightest pixel of the image has 42 counts for a 9.1-ks exposure. Note that the north-west quarter of the extended emission has less X-ray surface brightness than the rest and, at a PA $\sim$ 340 (north-north-west), a faint linear feature, corresponding to the north radio lobe and hot spot (see Hines & Wills 1993), is seen.

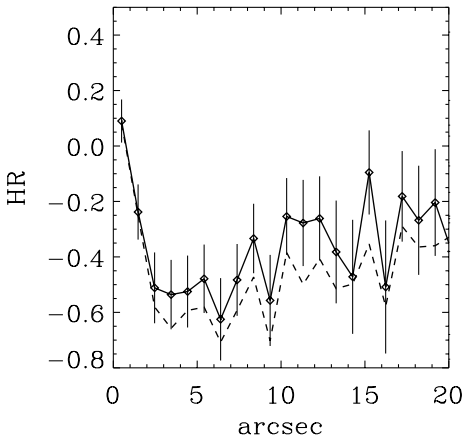

Figure 2. Radial profiles of hardness ratios, defined by HR = $(H-S)/(H+S)$, where H and S are integrated counts per unit area in the hard and soft bands, respectively. The solid line represents the hardness ratio for H in range 2–7 keV and S in range 0.3–0.8 keV, while the dashed line is for H in range 2–7 keV and S in range 0.8–2 keV. The x-axis is measured from the position of the nuclear point source and the profiles have been averaged azimuthally. Note the hard spectrum of the nuclear source.

3.2 X-ray spectrum of the central source

The spectral data of the central source were collected from a circular region with a 1-arcsec radius. Over 80 per cent of photons from a point source are expected to fall in this region. The count rate is $0.022\,\mathrm{count\,s^{-1}}$ in the 0.6–7 keV band and the spectrum is shown in Fig. 3. A prominent feature in the spectrum is the strong line at 4.5 keV on the hard excess emission, which is identified with Fe Kα at a rest energy of 6.4 keV.

The hard component above 3 keV can be described by a power law absorbed by $N_{\rm H} \sim 3 \times 10^{23}\,\mathrm{cm^{-2}}$ when a reasonable photon index is assumed (e.g. $\Gamma = 2$). However, extrapolating this model to higher energies fails to explain the *BeppoSAX* detected flux at 20–30 keV by a factor of $\sim$30. We therefore rule out the possibility of an absorbed continuum and attribute this component to a reflection continuum from cold matter. This interpretation is more favourable also on account of the strong Fe K line. The XSPEC model, `pexrav` (Magdziarz & Zdziarski 1995), appropriate for a reflection spectrum from neutral matter, provides a good fit to the data apart from the Fe K line. For the illuminating source, a power-law spectrum with $\Gamma = 2$ and no high-energy cut-off is assumed. The quality of the fit is insensitive to the choice of the power-law slope in a reasonable range. The Fe K line is found at the rest energy of 6.40 ± 0.07 keV. The line width is 60^{+150}_{-60} eV in Gaussian dispersion and the line intensity is $7.2^{+6.1}_{-3.3} \times 10^{-6}\,\mathrm{photon\,s^{-1}\,cm^{-2}}$, corresponding to a redshift-corrected equivalent width of $1.1^{+0.9}_{-0.5}$ keV. Note that the Fe K line of the cluster gas is at a clearly higher energy at $\sim$6.7 keV.

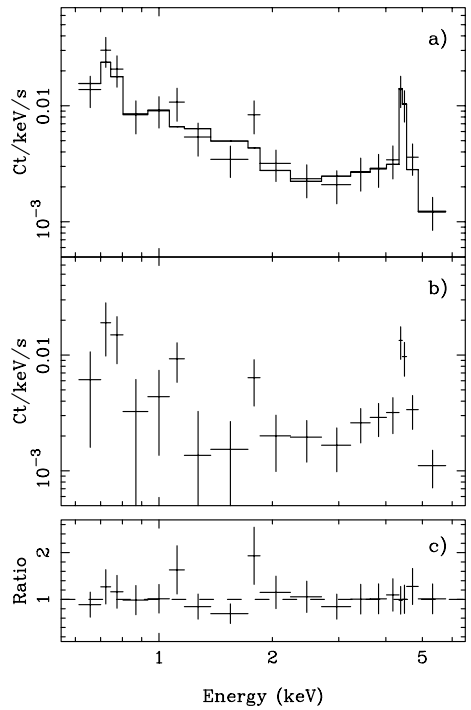

Figure 3. The *Chandra* ACIS-S spectrum of the central source of IRAS 09104+4109: (a) the data with no background subtraction, and fitted with a model consisting of the thermal emission model, cold reflection continuum (`pexrav`) and a Gaussian; (b) the same data as (a) but subtracting the data taken from the $1 \leqslant r \leqslant 2$ arcsec annulus normalized by geometrical area; (c) the residual of the fit given in (a) represented by the ratio between the data and the model. A strong line feature seen at 4.5 keV is a redshifted Fe Kα line (6.4 keV), which has an equivalent width of $\sim$1 keV with respect to the hard continuum.

Below 2 keV, a steep rise is seen in the spectrum towards lower energies. The spectrum in this energy range is sensitive to the background subtraction. The cluster emission increases its surface brightness steeply towards the centre, which makes an accurate estimate of the contribution from the cluster to the nuclear spectrum difficult. If no background is subtracted, the soft X-ray emission can be described by the thermal emission model, MEKAL, with a temperature of $kT = 1.7^{+0.8}_{-0.3}$ keV and Solar metallicity (Fig. 3a). Higher metallicity (2–$3\,\mathrm{Z_\odot}$) is favoured by the data when metallicity is left as a free parameter, although the constraint is rather loose. No excess absorption above the Galactic value ($N_{\rm H} \simeq 1.8 \times 10^{20}\,\mathrm{cm^{-2}}$, Dickey & Lockman 1990; Murphy et al. 1996) is required. The temperature is significantly lower than the cluster emission near the nucleus ($kT \approx 3.3$ keV). This suggests that a softer spectrum of the nuclear source composes a significant fraction in the energy range. This is supported by the fact that the soft X-ray image shows a narrow peak at the same position as the hard X-ray peak. The excess of the nuclear emission, in fact, appears to be largely the result of strong emission lines, particularly a strong feature at 0.75 keV ($\sim$1.1 keV in the rest frame and arising from the Fe L complex and ionized Ne). If the background data are taken from an annulus of the immediate surroundings ($1 \leqslant r \leqslant 2$ arcsec in radii), subtracting this background has no effect on the spectrum above 3 keV, but reduces the count rate in the 0.6–2 keV band by 44 per cent and leaves possible emission features (Fig. 3b). This soft X-ray emission could be the emission from photoionized gas at the inner nucleus. However, we tentatively fit the data with no background to the thermal emission model here and will discuss the origin in the Discussion section.

A spectral fit with the components described above is shown in Fig. 3(a), where the resulted χ^2 value is 8.5 for 14 degrees of freedom (Fig. 3c). Placing a reasonable amount of absorption (a few times of $10^{21}\,\mathrm{cm^{-2}}$ in $N_{\rm H}$, e.g. equivalent absorption to the NLR reddening) on the reflection component does not make any significant difference in the quality of the overall fit or spectral parameters of the thermal component. The observed 0.5–7 keV flux is estimated to be $2.5 \times 10^{-13}\,\mathrm{erg\,cm^{-2}\,s^{-1}}$, which can be translated to the rest-frame 0.7–10 keV luminosity of $6 \times 10^{43}\,h^{-2}\,\mathrm{erg\,s^{-1}}$.

4 COMPARISON WITH THE *BEPPOSAX* DATA

The *BeppoSAX* PDS data (14–40 keV range) were taken from the archive to compare with the *Chandra* data. Franceschini et al. (2000) attributed the hard X-ray emission detected with the *BeppoSAX* PDS to a strongly absorbed, transmitted component. Using the spectral fit to the *Chandra* data, we find that this conclusion depends on the assumed spectral slope of the source illuminating the reflecting matter. Given the low signal-to-noise ratio of the PDS data, no good constraints can be obtained for the spectral slope, however. We thus show only two cases of $\Gamma = 2$ and $\Gamma = 1.4$ for a primary source spectrum.

When $\Gamma = 2$, typical for a quasar, is assumed, even with an almost face-on setting of the reflection slab in the `pexrav` model (which yields the hardest spectrum above 10 keV), the PDS data lie a factor of $\sim$5 above the extrapolation of the cold reflection model for the *Chandra* nuclear spectrum. This suggests the presence of an extra high energy component arising from transmitted radiation, as proposed by Franceschini et al. (2000). If an absorbed power law is fitted to this excess component, the best-fitting value of the column density is found to be $3.3 \times 10^{24}\,\mathrm{cm^{-2}}$ (cf. Franceschini et al. 2000 obtained $6.6 \times 10^{24}\,\mathrm{cm^{-2}}$).

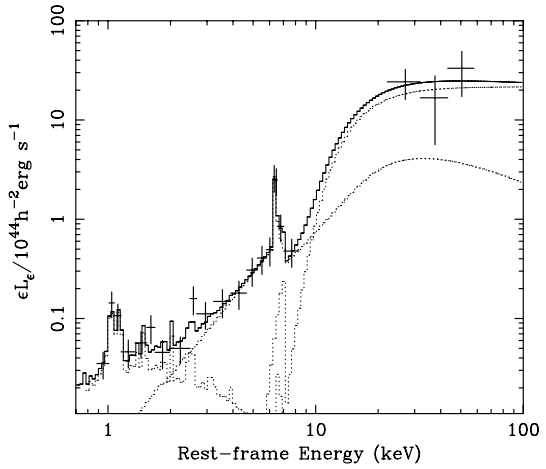

Figure 4. The *Chandra* data of the nuclear source of IRAS 09104+4109 and the *BeppoSAX* PDS data with the best-fitting model (solid histogram) consisting of thermal emission, cold reflection and highly absorbed emission components (dotted line histograms). The values of the data and model have been converted to those of luminosity. The energy scale has been corrected for the redshift of the galaxy.

We note a large statistical error in the $N_{\rm H}$ value and further ambiguities arising from Compton scattering and iron metallicity in such a high column density range (Matt, Pompilio & La Franca 1999; Wilman & Fabian 1999). Despite all the uncertainties, the Thomson depth of the X-ray absorber should exceed unity. The apparent lack of the transmitted component in the *Chandra* energy range sets the lower limit of the column density to be $2\times10^{24}\,{\rm cm}^{-2}$, while the detection of the hard X-ray excess means $N_{\rm H}$ is no larger than $10^{25}\,{\rm cm}^{-2}$. A joint fit to the *Chandra* ACIS and *BeppoSAX* PDS spectra with this model gives $\chi^2 = 10.0$ for 18 degrees of freedom (see Fig. 4).

In the case of $\Gamma = 1.4$, which is on the flatter side of the photon index distribution of quasars (e.g. Reeves & Turner 2000), the PDS data are explained well by cold reflection best-fitting the ACIS data (as mentioned in the previous section, the quality of the fit to the ACIS data is not sensitive to the selection of slope) with $\chi^2 = 10.8$ for 20 degrees of freedom. In this case, no transmitted component is required and the column density of the X-ray absorber exceeds $10^{25}\,{\rm cm}^{-2}$.

5 DISCUSSION

5.1 Buried QSO

A distinctive cold reflection feature is observed from the nucleus of IRAS 09104+4109 in the *Chandra* spectrum whilst no primary radiation is visible. Detection of the primary emission at higher energies with *BeppoSAX* (Franceschini et al. 2000) depends, as demonstrated above, on the assumed spectrum of the source.

If the PDS-detected X-rays are entirely the result of reflection, only a lower limit of the primary source luminosity can be obtained, which is a minimum requirement to produce the observed luminosity through cold reflection. The albedo (η) in the 2–10 keV band is calculated using the `pexrav` model for two inclination angles, $i = 20°$ and 60°, for the reflecting slab subtending 2π in solid angle. For $\Gamma = 1.4$, $\eta = 0.066$ ($i = 20°$) and 0.052 ($i = 60°$). Therefore the luminosity of the primary source is larger than $5\times10^{43}\eta^{-1} \simeq 7.6\times10^{44}\,{\rm erg\,s^{-1}}$ and $9.6\times10^{44}\,{\rm erg\,s^{-1}}$ for the respective inclinations. As the fraction of reflecting surface visible to us is likely to be less than unity, the true luminosity of the primary source should be larger than these values.

We discuss below the case in which the primary source has a power law of $\Gamma = 2$ and hence its transmitted radiation is detected with the PDS. The 2–10 keV luminosity of the primary source corrected for the absorption (and effects of Compton scattering, Matt et al. 1999) is estimated to be $7.4\times10^{45}\,\gamma h^{-2}\,{\rm erg\,s^{-1}}$ ($\gamma \sim 1$ for a spherical obscuration, and it can go up to $\sim$3 if absorption occurs at a small cloud in the line of sight when $N_{\rm H} = 3\times10^{24}\,{\rm cm}^{-2}$). The observed-to-intrinsic luminosity ratio in the 2–10 keV band is then $0.67\gamma^{-1}$ per cent for IRAS 09104+4109. If the ratio of the 2–10 keV to bolometric luminosities is assumed to be $f_{\rm HX/Bol} = 0.05 f_{\rm HX/Bol,0.05}$, typical for quasars (e.g. Elvis et al. 1994), the bolometric luminosity is $1.5\times10^{46} f_{\rm HX/Bol,0.05}^{-1}\,\gamma h^{-2}\,{\rm erg\,s^{-1}}$. This is comparable to $L_{\rm ir} = 2.3\times10^{46}\,h^{-2}\,{\rm erg\,s^{-1}}$, and consistent with a picture where the bulk of the infrared emission is powered by a buried quasar through dust reradiation. The radio source has an intermediate power between FR I and FR II (Kleinmann et al. 1988; Hines & Wills 1993). However, without the nuclear obscuration, the wide-band energy distribution of IRAS 09104+4109 would be closer to that of radio-quiet AGNs.

The cold gas reflecting the observed X-rays is probably part of the clouds occulting the central source. An X-ray absorber with as large a column density as is found in IRAS 09104+4109 is likely to be compact, probably parsec-scale in radius, as for nearby Compton-thick Seyfert 2 galaxies (Matt 2000). The flat energy distribution in the infrared band indicates that hot dust at near sublimation temperature ($\sim$1000 K) is present and the inner radius of the dusty torus is of the order of 1 pc (Granato et al. 1996; Taniguchi et al. 1997). The mid-infrared spectrum obtained from ISOCAM CVF (Taniguchi et al. 1997) fits well with the compact dusty torus model of Pier & Krolik (1992) with an edge-on view (also see Granato & Danese 1994; Granato et al. 1996), whereas optical polarization studies imply a moderately inclined torus (Hines et al. 1999; Tran et al. 2000). The characteristic dust temperature is about 120 K (e.g. Kleinmann et al. 1988). No *IRAS* detection at 100 μm and the new SCUBA limit at 850 μm (Deane & Trentham 2001) rule out the presence of cool dust, which is a common feature of local ultraluminous infrared galaxies (ULIGs). No detection of CO (Evans et al. 1998) is consistent with a relatively small obscuring torus with a modest mass. A large covering factor ($\geqslant$0.9) is favoured by all the observations.

The soft X-ray emission seen in the nuclear spectrum is probably caused by photoionized gas in the inner nucleus. The highly polarized biconical reflection nebula imaged by the *Hubble Space Telescope* (*HST*) (Hines et al. 1999) is, however, not a likely source, as scattering by dust rather than electrons appears to be a dominant mechanism to induce the high polarization (Tran et al. 2000). The inner wall of the obscuring torus is exposed to the intense radiation from the primary source and thus expected to be highly ionized. Provided the optical depth of the ionized gas is small, the Fe L emission bump can be very strong (e.g. Band et al. 1990). A sub-pc scale ionized disc has indeed been imaged with the Very Large Baseline Array (VLBA) in the nucleus of the nearby Compton-thick Seyfert 2 galaxy NGC 1068 (Gallimore, Baum & O'Dea 1997), and they predicted strong soft X-ray emission lines based on a photoionization computation. In this case, the luminosity of the emission from the photoionized gas should be larger than observed ($\sim3\times10^{42}\,h^{-2}\,{\rm erg\,s^{-1}}$ in the 0.5–2 keV band), as significant absorption is likely to occur during the escape from the nuclear region.

A possible alternative is hot stars near the nucleus, inferred from a Wolf–Rayet feature seen in the optical spectrum of the nuclear region (Tran et al. 2000). However, the luminosity of this component alone is one order of magnitude more luminous than the nearby Wolf–Rayet galaxies observed with *ROSAT* (Stevens & Strickland 1998), and the high metallicity implied from the strong emission-line features is also unusual (but see Buote 2000).

5.2 Implications for other luminous IR galaxies

IRAS 09104+4109 is so far the only hyperluminous infrared galaxy detected in X-rays (apart from PG1634 + 706 which is an unobscured quasar, see Nandra et al. 1995 for the *ASCA* result), and the most distant reflection-dominated spectrum X-ray source known with a clear detection of the Fe K line. The small X-ray reflection fraction ($\sim$0.7 per cent in the 2–10 keV band; $\sim$0.1 per cent at the rest energy of 2 keV) estimated for IRAS 09104+4109 is still consistent with the limit obtained from the previous observations for other luminous infrared galaxies at high redshift (see Fabian et al. 1996; Ogasaka et al. 1997 for F15307+3252; Wilman et al. 1998). *Chandra* and *XMM* are capable of detecting reflected X-ray light from F15307+3252, if the reflection fraction is similar to that of IRAS 09104+4109. Although a 2σ detection of the lensed object IRAS F10214+4724 with *ROSAT* HRI was reported (Lawrence et al. 1994), an 80 ks *ASCA* observation failed to detect it. The prospect of X-ray detection of this object depends on the lensing geometry. It should be noted that IRAS 09104+4109 is peculiar among the ULIG population being in a cluster environment, and how common this type of objects is unclear (e.g. Deane & Trentham 2001).

Chandra observations of the SCUBA sources have revealed no correlation between the submillimetre and X-ray source populations (Fabian et al. 2000b; Hornschemeier et al. 2000), with two exceptions (Bautz et al. 2000). If ULIGs at high redshift are powered predominantly by AGNs, as suspected by Trentham, Blain & Goldader (1999); Trentham (2001), their nucleus is Compton-thick and the X-ray reflection fraction is indeed as low as that in IRAS 09104+4109. On the other hand, the sources with a small X-ray optical depth, which are preferably detected in X-rays, may tend to have hotter dust (Wilman, Fabian & Gandhi 2000), which deters submillimetre detection.

ACKNOWLEDGMENTS

We thank all the members of the *Chandra* team for building and operating the satellite and developing the data analysis software. Neil Trentham, Steve Allen and Carolin Crawford are thanked for helpful discussion. The Royal Society (ACF, SE) and PPARC (KI) are thanked for support.

REFERENCES

Allen S. W., Fabian A. C., 1998, MNRAS, 297, L57
Armus L., Soifer B. T., Neugebauer G., 1999, Ap&SS, 266, 113
Band D. L., Klein R. I., Castor J. I., Nash J. K., 1990, ApJ, 362, 90
Bautz M. W., Malm M. R., Baganoff F. K., Ricker G. R., Canizares C. R., Brandt W. N., Hornschemeier A. E., Garmire G. P., 2000, ApJ, 543, L119
Buote D., 2000, ApJ, 539, 172
Celotti A., Ghisellini G., Chiaberge M., 2001, MNRAS, in press
Crawford C. S., Vanderriest C., 1996, MNRAS, 283, 1003
Deane J., Trentham N., 2001, MNRAS, submitted
Dickey J. M., Lockman F. J., 1990, ARA&A, 28, 215
Elvis M. et al., 1994, ApJS, 95, 1
Ettori S., Fabian A. C., 1999, MNRAS, 305, 834
Evans A. S., Sanders D. B., Cutri R. M., Radford S. J. E., Surace J. A., Solomon P. M., Downed D., Kramer C., 1998, ApJ, 506, 205
Fabian A. C., Crawford C. S., 1995, MNRAS, 274, L63
Fabian A. C. et al., 1994, ApJ, 436, L51
Fabian A. C., Cutri R. M., Smith H. E., Crawford C. S., Brandt W. N., 1996, MNRAS, 283, L95
Fabian A. C. et al., 2000a, MNRAS, 318, L65
Fabian A. C. et al., 2000b, MNRAS, 315, L8
Franceschini A., Bassani L., Cappi M., Granato G. L., Malaguti G., Palazzi E., Persic M., 2000, A&A, 353, 910
Frontera F., Costa E., dal Fiume D., Feroci M., Nicastro L., Orlandini M., Palazzi E., Zavattini G., 1997, Proc. SPIE, 3114, 206
Gallimore J. F., Baum S. A., O'Dea C. P., 1997, Nat, 388, 852
Granato G., Danese L., 1994, MNRAS, 268, 235
Granato G., Danese L., Franceschini A., 1996, A&A, 460, L11
Hines D. C., Wills B. J., 1993, ApJ, 415, 82
Hines D. C., Schmidt G. D., Wills B. J., Smith P. S., Sowinski L. G., 1999, ApJ, 512, 145
Hornschemeier A. E. et al., 2000, ApJ, 541, 49
Hutchings J. B., Neff S. G., 1988, AJ, 96, 1575
Kleinmann S. G., Hamilton D., Keel W. C., Wynn-Williams C. G., Eales S. A., Becklin E. E., Kuntz K. D., 1988, ApJ, 328, 161
Lawrence A., Rigopoulou D., Rowan-Robinson M., McMahon R. G., Broadhurst T., Lonsdale C. J., 1994, MNRAS, 266, L41
McNamara B. R. et al., 2000, ApJ, 543, L135
Magdziarz P., Zdziarski A., 1995, MNRAS, 273, 837
Matt G., 2000, A&A, 355, L31
Matt G., Pompilio F., La Franca F., 1999, New Astron., 4, 191
Murphy E. M., Lockman F. J., Laor A., Elvis M., 1996, ApJS, 105, 369
Nandra K., Fabian A. C., Brandt W. N., Kunieda H., Matsuoka M., Mihara T., Ogasaka Y., Terashima Y., 1995, MNRAS, 276, 1
Ogasaka Y., Inoue H., Brandt W. N., Fabian A. C., Kii T., Nakagawa T., Fujimoto R., Otani C., 1997, PASJ, 49, 179
Pier E., Krolik J. H., 1992, ApJ, 401, 99
Reeves J. N., Turner M. J. L., 2000, MNRAS, 316, 234
Soifer B. T., Neugebauer G., Armus L., Shupe D. L., 1996, AJ, 111, 649
Stevens I. R., Strickland D. K., 1998, 294, 523
Taniguchi Y., Sato Y., Kawara K., Murayama T., Mouri H., 1997, A&A, 313, L1
Tran H. D., Cohen M. H., Villar-Martin M., 2000, AJ, 120, 562
Trentham N., 2001, MNRAS, in press (astro-ph/0004370)
Trentham N., Blain A. W., Goldader J., 1999, MNRAS, 305, 61
Weisskopf M. C., O'Dell S. L., van Speybroeck L., 1996, Proc. SPIE, 2805, 2
Wilman R. J., Fabian A. C., 1999, MNRAS, 309, 862
Wilman R. J., Fabian A. C., Cutri R. M., Crawford C. S., Brandt W. N., 1998, MNRAS, 300, L7
Wilman R. J., Fabian A. C., Gandhi P., 2000, MNRAS, 318, L11

This paper has been typeset from a TEX/LATEX file prepared by the author.